International Journal of Fatigue 43 (2012) 226–234

Contents lists available at SciVerse ScienceDirect

International Journal of Fatigue

journal homepage: www.elsevier.com/locate/ijfatigue

A non-linear damage evolution model for mode II fatigue delamination onset and growth

G. Allegri *, M.R. Wisnom

Advanced Composites Centre for Innovation and Science (ACCIS), University of Bristol, University Walk, BS8 1TR Bristol, UK

ARTICLE INFO

Article history:
Received 14 November 2011
Received in revised form 12 March 2012
Accepted 16 March 2012
Available online 19 April 2012

Keywords:
Fatigue modelling
Composites
Crack growth rate
Cumulative damage

ABSTRACT

A novel approach is proposed describing both the onset and growth of delaminations in fibre-reinforced laminates under pure mode II constant amplitude loading with the same damage evolution rule, unifying these two aspects of the material behaviour that are normally treated separately. A scalar damage variable is introduced to represent the fraction of overall fatigue endurance used up at ply interfaces as a function of the number of accumulated cycles. The damage rate equation is postulated in a generic power law format, which also includes the effect of the load stress-ratio. The material SN curves for pure mode II loading are obtained in closed form by a simple integration of the assumed damage evolution law. The material delamination propagation rate as a function of the energy release rate and the stress-ratio is similarly obtained combining the aforementioned damage evolution law with a regularized expression for the stress field at the crack tip. Two independent fatigue related parameters are sufficient for describing both the delamination onset and its growth. This modelling approach is validated by means of experimental fatigue delamination data for IM7/8552 carbon fibre/epoxy, demonstrating that the unified modelling strategy is able to describe both fatigue initiation and propagation and the associated effect of the stress-ratio.

1. Introduction

The fatigue damage accumulation in composite materials starts with micro-cracking in off-axis plies and evolves into the onset and growth of delaminations, which is finally followed by extensive fibre failure leading to structural collapse [1]. Each of these damage mechanisms occurs at a characteristic length scale and requires "ad hoc" modelling tools in order to be consistently described. Therefore there exists a vast literature addressing the various aspects of the phenomenology of damage accumulation in fibre-reinforced composites and its physical description.

Matrix cracking usually occurs in the very early stages of the fatigue life of composites, whilst fibre failure represents a relatively short final damage accumulation phase. Therefore the delamination onset and propagation typically constitutes the largest portion of the fatigue endurance of composite structural elements [2]. This is also because several features of fibre-reinforced laminates, such as free edges and ply drop-offs, act as interlaminar stress raisers which promote the onset and growth of delaminations.

It has been demonstrated that the fatigue delamination propagation is driven by the energy release rate (ERR) at the crack tip [3]. Therefore fracture mechanics and semi-empirical delamination propagation laws are the primary engineering tools for assessing the propensity of interlaminar cracks to grow from existing flaws. This constitutes the basis of a "damage tolerance" design approach for fatigue mitigation [4] in composites. Unfortunately the slope of the delamination propagation rate versus ERR for state-of-the-art fibre-reinforced laminates is considerably steeper than that featuring cracks in metals. Thus if large scale fatigue delamination occurs in composite components, there is the potential for sudden catastrophic failures.

Thus the certification of primary composite structures, especially in the aerospace field, is usually based on "no growth" criteria for delaminations emanating from stress raisers, such as the aforementioned ply drop-offs or free-edges, or initial internal defects such as voids, gaps and overlaps. "No growth" criteria are expressed in a quantitative fashion via curves relating the number of cycles for the delamination "initiation" to the ERR locally attained. Strictly speaking "initiation" is a misnomer in a "no growth" approach, since the very fact that an ERR measure is employed implies that the damage has already occurred in a discrete form, e.g. as short interlaminar cracks in the case of delamination. Moreover, some amount of propagation must occur in order to detect any change of the delamination size with respect to the initial assumed damage pattern, as recognised also in the current testing standards [5]. Usually the amount of effective propagation associated with "no growth" criteria is in the range of a few millimetres

* Corresponding author. Tel./fax: +44 0 1234750111.
E-mail address: giuliano.allegri@bristol.ac.uk (G. Allegri).

0142-1123/$ - see front matter © 2012 Elsevier Ltd. All rights reserved.
http://dx.doi.org/10.1016/j.ijfatigue.2012.03.016

for coupon level testing. At a structural level the size of detectable delamination is often much larger due to the intrinsic limitations of non-destructive inspection techniques. However the key point is that "no growth" criteria map onto "damage tolerance" delamination growth rates as functions of ERR in the near threshold regime [4].

"Initiation" in a proper sense takes place when damage of some sort appears in an initially pristine material because of localised stress raisers. In a "safe life" design, initiation cannot take place until the end of the operative life. "Initiation" is essentially strength dependent and so engineering SN curves are the appropriate tool for the "safe life" design of composite elements [6]. In structural engineering SN curves are described using the well-established Basquin's power law [7], that has been found to govern the fatigue endurance of a wide class of structural materials.

In order to predict the onset and growth of fatigue damage in fibre-reinforced composites, several phenomenological models have been proposed in the past. According to the comprehensive review authored by Degrieck and Van Paepegem [8] these can be classified into fatigue life models, stiffness/strength degradation models and progressive damage models. The first two classes of models have been developed for fatigue damage onset and are usually based on equivalent stress or strain measures [9–11]. Progressive damage models [12–15] account for the presence of a flaw having a finite size, e.g. a delamination in an interface, and aim to predict the defect propagation as a function of the number of fatigue cycles applied. Since according to linear elastic fracture mechanics (LEFMs) the stress field and strain fields are singular at the tip of the crack, progressive damage models identify the energy release rate (ERR) as the physical agent driving the crack propagation. Therefore, following LEFM, stress based models are suitable only for describing the onset of discrete damage, e.g. delamination, whilst fracture mechanics has to be employed whenever a flaw having finite size occurs.

Mandell and Meier [16] experimentally characterised the fatigue propagation of mode I in-plane cracks in brittle carbon epoxy cross-ply laminates. They observed that the 90° plies developed an array of uniformly spaces splits ahead of the 0° layers fracture tips. These splits were perpendicular to the 0° ply cracks, effectively inducing tip blunting and thus reducing the effective stress concentration. The 0° cracks advanced in a sequence of discrete steps, progressively fracturing the ligaments between the ply splits in the 90° plies, as qualitatively illustrated in Fig. 1. In other words the in-plane crack was bridged by the ligaments created in the split 90° plies. LEFM would dictate that the normal stress σ is singular at the crack tip, i.e. following the classical relation

$$\sigma = K_I/\sqrt{2\pi r} \tag{1}$$

where K_I is the stress intensity factor (SIF) and r the distance from the crack tip along the direction of propagation. Contrary to LEFM, due to the bridging action exerted by the ligaments in the 90°, Mendell and Meier [16] assumed that within a distance r_c from the crack tip the normal stress attained the constant value

$$\sigma = \sigma_f K_I/K_{IC} \tag{2}$$

where σ_f is the material un-notched tensile strength and K_{Ic} the material fracture toughness.

The radius of the constant stress region near the crack tip is determined by the condition that the LFEM normal stress from Eq. (1) corresponding to the material fracture toughness exceeds the material un-notched strength; this yields

$$r_c = \frac{K_{Ic}^2}{2\pi\sigma_f^2} \tag{3}$$

In Eq. (2) the definition of the SIF K_I is still that dictated by LEFM. Eq. (2) implies that the material fails at the crack tip when the un-notched static strength is attained and this occurs when the LEFM SIF equals the material toughness. This assumption allows to relate in a simple fashion the strength and fracture properties and was also proven to be in agreement with experimental data obtained from in-plane cracked coupons [16].

Andersons et al. [17] suggested that, despite the complexities associated with the inhomogeneous nature of interfaces, local crack bridging and material anisotropy, the propagation of delaminations can be described as a sequence of initiation, i.e. onset, steps taking place in the neighbourhood of the interlaminar crack tip. In order to represent the stress field at the crack tip they proposed a mixed-mode extension of the de-singularized stress field originally proposed by Mandell and Meier [16] and given in Eq. (2). This allowed them to derive a semi-empirical mixed-mode fatigue growth law for brittle composites, which also describes the effect of the applied stress-ratio.

In the present study, the delamination propagation is still considered as a superposition of initiation steps at the micro-scale, but a general damage evolution rule is introduced to derive both the proper "initiation" SN curves in pure shear and a semi-empirical equation for mode II interlaminar crack growth. In order to obtain the latter, the stress at the crack tip is de-singularized as proposed by Mandell and Meier. In-plane matrix micro-cracking, ply-splitting and fibre failure are not accounted for in this analysis, so the emphasis is here placed only on damage that occurs in the form of delamination.

2. Damage evolution

2.1. General considerations

Let xz be one of the three principal orthotropy planes of a composite laminate and let such a plane be in a state of plane stress. Let E_x be the pristine laminate equivalent Young's modulus in the x direction shown in Fig. 1, E_z be the equivalent Young's modulus in the z direction, i.e. through-the-thickness, G_{xz} shear modulus in the xz plane and ν_{xz} the through-thickness Poisson's ratio. The aforementioned moduli are "equivalent" in the sense that they are obtained via a standard stacking sequence homogenisation based on classical laminate theory; at ply level, the material is assumed homogenous. Considering a mode II, i.e. pure shear, crack in the x direction, the following relation holds between the stress intensity factor K_{II} and the energy release rates G_{II} [18]

$$G_{II} = \alpha_{II} K_{II}^2 \tag{4}$$

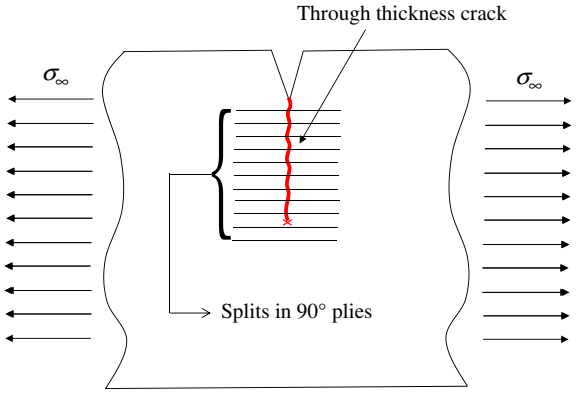

Fig. 1. Crack tip blunting due to ply splitting as observed by Mandell and Meier [16].

where

$$\alpha_{II} = \lambda^{1/4}\sqrt{\frac{1+\rho}{2E_xE_z}} \tag{5}$$

and

$$\lambda = \frac{E_z}{E_x} \quad \rho = \sqrt{E_xE_z}\left(\frac{1}{2G_{xz}} - \frac{\nu_{xz}}{E_x}\right) \tag{6}$$

Eqs. (1)–(3) still hold in a plane strain case, but the equivalent elastic moduli must be calculated via the plane strain material compliance coefficients [19]. It is here assumed that the material is homogeneous, so E_x, E_z, ν_{xz} and G_{xz} are constants.

Let a pristine interface in the laminate be subjected to an alternating shear stress having local peak value $\tau_{\max}(x)$ and stress-ratio R, where x is a coordinate along an arbitrary ply interface. The load severity for a pristine interface is here defined as the ratio between the peak stress $\tau_{\max}(x)$ and the un-notched material static shear strength τ_u, i.e. $\tau_{\max}(x)/\tau_u$. Since the material is considered homogeneous, also τ_u is here considered constant.

If the interface is delaminated, by adopting the Mandell and Meier assumption, one obtains a finite value for the peak shear stress $\tau_{\max}(x)$ for $0 \leqslant r < r_c$. By analogy with Eq. (2), the latter can be expressed as follows

$$\tau_{\max} = \tau_u \frac{K_{II\max}}{K_{IIc}} = \tau_u\sqrt{\frac{G_{II\max}}{G_{IIc}}} \tag{7}$$

where the relation between the mode II SIF and ERR given in Eq. (4) has been employed. In Eq. (7) $K_{II\max}$ and $G_{II\max}$ are respectively the peak SIF and ERR associated with a fatigue cycle. Therefore for a delaminated interface the load severity is given by $\sqrt{\frac{G_{II\max}}{G_{IIc}}}$ for $0 \leqslant r < r_c$. In analogy with Eq. (3) the radius of the constant stress region for a pure mode II delamination is given by

$$r_c = \frac{G_{IIc}}{2\pi\alpha_{II}\tau_u^2} \tag{8}$$

Outside the constant stress region, i.e. $r \geqslant r_c$, the shear distribution is that provided by LEFM

$$\tau_{\max} = \sqrt{\frac{G_{II\max}}{2\pi\alpha_{II}r}} \tag{9}$$

The shear field described by Eqs. (7) and (9) will be from now on denoted as Mendell and Meier stress field.

The rationale for adopting the Mandell and Meier stress field in the context of mode II delamination propagation is provided by the following reasoning. As sketched in Fig. 2, one can observe that the stress field ahead of a sharp tip will be pure tension at an angle of 45° with respect to the interlaminar crack growth direction. O'Brien [20] reported that voids grow at the interface of mode II delamination in relatively brittle epoxies under the principal tensile stress field and then those flaws coalesce into shear hackles. It is clear that, from a geometrical point, the otherwise sharp crack tip is rounded by such voids, so a blunt crack tip stress model, as the one proposed by Mandell and Meier, should be adequate to describe the fatigue damage accumulation process in mode II. However care must be exercised in extending such conclusions to different mode-mixity values, whereby the crack blunting mechanism might not occur.

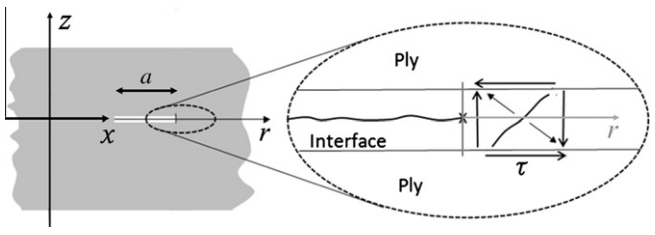

Fig. 2. Interface delamination with sharp tip.

2.2. Non-linear damage evolution law

The progressive onset of a delamination within the laminate ply stack is here represented by introducing a scalar damage field $D(x) \in [0,1]$, where x is a coordinate spanning an arbitrary ply interface. In this paper $D(x)$ represents the ratio of the number of cycles $\Delta N\left[R, \frac{\tau_{\max}(x)}{\tau_u}\right]$ accumulated at the location x in an interface subjected to an alternating shear stress having constant local severity $\frac{\tau_{\max}(x)}{\tau_u}$ and stress-ratio R to the total number of fatigue cycles $N_f\left[R, \frac{\tau_{\max}(x)}{\tau_u}\right]$ that can be withstood at the location x prior to failure, i.e. the interface fatigue endurance for the load regime represented by $\frac{\tau_{\max}(x)}{\tau_u}$ and R. In mathematical terms

$$D(x) = \frac{\Delta N\left[R, \frac{\tau_{\max}(x)}{\tau_u}\right]}{N_f\left[R, \frac{\tau_{\max}(x)}{\tau_u}\right]} \tag{10}$$

The damage field given in Eq. (10) is the based on the "endurance based" definition of damage introduced by Chaboche [21] for alloys. It is worth remarking that since such definition is purely endurance based, it does not imply the presence of material stiffness degradation mechanisms. Therefore the elastic moduli which appear in Eqs. (4), (5) must be independent from the damage evolution and accumulation processes. This is in full agreement with the basic postulates of LEFM, which does not imply any change of the mechanical properties of the material in the neighbourhood of the delamination tip. This is also consistent with the introduction of the Mendell and Meier de-singularized shear stress field given in Eqs. (7) and (9). Such field implies that the material at the delamination tip stays linear elastic when damage is accumulated, because the crack tip blunting is a purely geometrical effect.

It is natural to assume $D(x) = 0$ for a pristine material, while $D(x) = 1$ when the number of cycles to failure $N_f\left(R, \frac{\tau_{\max}}{\tau_u}\right)$ has been reached. Since $D(x)$ is scalar, it is in principle suitable for representing only relatively diluted isotropic flaw distributions [22]. It is also possible to account for the initial presence of defects or pre-fatigue environmental degradation in the material at the start of the fatigue life by introducing a non-zero initial damage value.

The damage evolution law for any location x within a pristine interface is here postulated in differential form, i.e. assuming that the damage increment per unit fatigue cycle can be expressed as follows

$$\frac{dD(x)}{dN} = \frac{[1-D(x)]^{-p}}{(p+1)}\left[\frac{\tau_{\max}(x)}{\tau_u}\right]^{\frac{b}{(1-R)^{\kappa}}} \tag{11}$$

where p, b and κ are nondimensional material dependent parameters. These must be identified by suitable fatigue tests. As stated in Section 2.1, it is hereby assumed that the material is homogeneous, so p, b and κ are independent from the coordinate x spanning the interface. It is also assumed that $p > 0$, $b > 0$ and $\kappa > 0$. In the remainder of this paper p, b and κ will be referred to as "material fatigue parameters". It is therefore assumed that the elastic moduli E_x, E_z, ν_{xz}, G_{xz} and the static un-notched shear strength τ_u are known from previous static tests. In Section 3 it will be demonstrated that the characteristic slope of the material SN curves in double logarithmic axes for shear driven delamination initiation in fibre-reinforced plastics is given by $-\frac{(1-R)^k}{b}$. Then in Section 4 it will be demonstrated that the slope of the delamination growth rate $\frac{da}{dN}$ versus the

normalised mode II ERR $\frac{G_{II\max}}{G_{IIc}}$ is given by $\frac{b}{2(1-R)^{\kappa}}$. Therefore only two material fatigue parameters, namely b and κ, are sufficient to describe both fatigue delamination initiation and growth in mode II. From an application point of view, this implies that delamination growth can be predicted from initiation tests and vice versa. This allows significantly reducing the amount of testing to be carried out in order to characterise the interlaminar fatigue behaviour of fibre-reinforced plastics.

Eq. (11) belongs to the general class of non-linear damage evolution laws with separable variables [22]. This implies that, as demonstrated in the Appendix, Eq. (11) leads to a linear damage accumulation law, namely the well established Miner's rule. More general degradation laws can be formulated introducing unseparable stress and damage variables [23]. This is usually done in order to obtain non-linear damage accumulation rules from non-linear damage evolution laws. The former have the advantage of being able to represent the sequence effects due to variable amplitude loading, which however are not considered in this paper.

The particular form chosen for Eq. (11) is formally analogous to that of several other stress-based phenomenological damage models proposed in the literature [9–11]. All such models postulated a power law dependency of the damage accumulation rate on either a strain or a stress measure, as in Eq. (11). Moreover in the literature the $dD(x)/dN$ expressions always comprise a term leading to an accelerating damage evolution rate, as the $[1-D(x)]^{-p}$ in the right hand side of Eq. (11). However there are two fundamental differences between Eq. (11) and other damage evolution laws presented in the literature: first the damage measure which appears Eq. (11) is purely endurance based, as originally proposed by Chaboche [21]. Secondly, the exponent of the stress term in Eq. (11) depends on the stress-ratio. The rationale and implications of such hypothesis will be discussed in detail in the following sections.

3. Delamination onset

Let x be a location within a pristine interface subjected to an alternating shear stress $\tau_{\max}(x)$ with stress-ratio R. Let $\tau_{\max}(x)$ be constant with respect to the number of fatigue cycles $N(x)$ accumulated. The number of cycles $N_f(x)$ required to produce failure of the interface at the location x to damage onset can be obtained via integrating Eq. (11) with the damage variable $D(x)$ ranging from zero, i.e. the pristine material case, to one, i.e. the completely failed interface scenario. The latter, i.e. $D(x) = 1$ for a given location within the interface corresponds to the onset of a delamination. Therefore one can write

$$\int_0^1 (1-D)^p dD = \frac{1}{(p+1)}\left[\frac{\tau_{\max}}{\tau_u}\right]^{\frac{b}{(1-R)^{\kappa}}} \int_0^{N_f} dN \tag{12}$$

In Eq. (12) the dependency from the spatial location x has been dropped for the sake of simplicity since the damage evolution at a single location in space is considered.

With the help of some elementary calculus Eq. (10) leads to

$$\frac{\tau_{\max}}{\tau_u} = N_f^{-\frac{(1-R)^{\kappa}}{b}} \tag{13}$$

Eq. (13) comprises only of two material dependent fatigue parameters introduced in Eq. (11), namely b and κ Eq. (13) represents the SN curve for interlaminar fatigue damage accumulation, i.e. the expression which relates the local applied stress level to the number of cycles at which the interface is completely failed at x. Eq. (11) has the form of a Basquin's type law [7], albeit the exponent is dependent on the stress-ratio R. For the sake of physical consistency it is worth observing that for static fracture one has $\tau_{\max} = \tau_u$, so from Eq. (13) the number of cycles to failure would be $N_f = 1$. Actually static failure would occur at a time during the first cycle, i.e. for a fractional value of N_f depending on the load waveform. This does not make any substantial difference in terms of engineering applications, so from this point onwards $N_f = 1$ will be regarded as the static fracture condition and vice versa.

As shown in Fig. 3a, the SN curves represented by Eq. (13) rotate anticlockwise in the $N_f - \tau_{\max}$ plane with respect to a pivot point that represents the static fracture condition, i.e. $N_f = 1$ and $\tau_{\max} = \tau_u$. In the limit $R \to 1$, the SN curves becomes horizontal. This is consistent from a physical point of view since for $R = 1$ the load becomes static, so no fatigue related degradation may occur. This characteristic trend has been already observed in the literature [24] and it is largely dependent on the visco-elastic nature of the fibre-reinforced matrix, which has a significant effect on the fatigue life even below the polymer glass transition temperature. In Section 5 it will be demonstrated that the assumed dependency of the stress term exponent in Eq. (11) on the stress-ratio is adequate for describing the SN curves generated by tests carried out at constant frequency, while retaining the linear elasticity hypothesis in terms of material behaviour.

4. Delamination growth

4.1. Shear stress at the delamination tip

As discussed in Section 1, it is here assumed that the delamination growth at the meso/macro-scale is essentially governed by initiation at the micro-scale, i.e. ahead of the interlaminar crack tip. In linear elasticity the shear stress field at the tip of a mode II crack is singular, but using the Mandell and Meier stress field from Eqs. (7) and (9) such singularity is suppressed. The qualitative trend of the Mandell and Meier stress field given by Eqs. (7) and (9) is presented in Fig. 4a, with the radius of the constant stress region r_c provided by Eq. (8). The fatigue delamination growth law is here obtained by integrating the damage produced by the de-singularized shear stress field shown in Fig. 4a along the interface. This implies considering the fatigue delamination propagation process as the superposition of initiation steps at the micro-scale.

4.2. Fatigue delamination growth law

Let r be the distance of a point belonging to a partially delaminated interface from the interlaminar crack tip, as shown in Fig. 2. Let the interface be subjected to alternating load and let $G_{II\max}$ the be the peak mode II ERR attained at the delamination tip during a fatigue cycle having stress-ratio R. The damage accumulation rate $\frac{dD(r)}{dN}$ along the bonded region of the interface is found by substituting the Mendell and Meier stress field given by Eqs. (7) and (9) into the damage evolution law postulated in Eq. (11). This yields

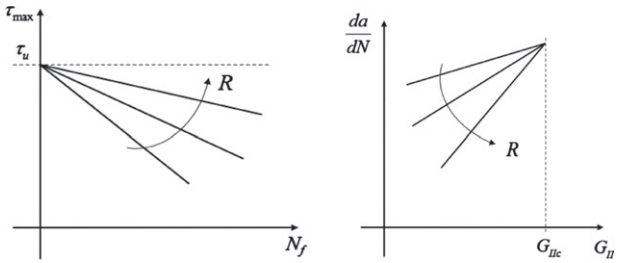

(a) SN curves from eq. (13) in double logarithmic axes

(b) Propagation curves from eq. (18) in double logarithmic axes

Fig. 3. Graphical representation of stress-ratio effect.

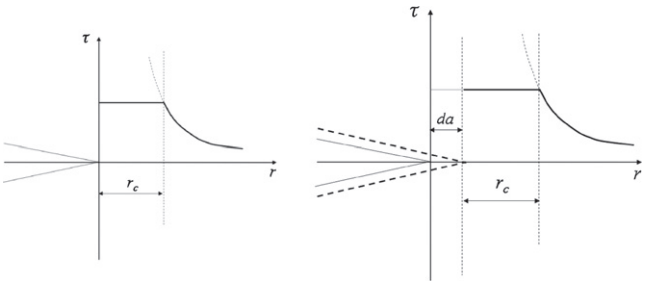

(a) Static, from Ref [16] (b) During propagation

Fig. 4. Mendell and Meier stress field at the delamination tip.

$$\frac{dD(r)}{dN}=\begin{cases}\frac{[1-D(r)]^{-p}}{(p+1)}\left[\frac{G_{II\max}}{G_{IIc}}\right]^{\frac{b}{2(1-R)^{\kappa}}} & r\leqslant r_c\\ \frac{[1-D(r)]^{-p}}{(p+1)}\left[\frac{G_{II}}{G_{IIc}}\frac{r_c}{r}\right]^{\frac{b}{2(1-R)^{\kappa}}} & r\geqslant r_c\end{cases} \tag{14}$$

The boundary conditions for the damage distribution given in Eq. (14) are the following

$$\lim_{r\to 0}D(r)=1\lim_{r\to\infty}D(r)=0 \tag{15}$$

The second of Eqs. (15) implies that the far field stress produces no damage in the material. This is a reasonable approximation since in this analysis it has been assumed that a single delamination is the dominant defect. In principle the boundary condition in the second of Eqs. (15) would take a different form in case of multiple interacting interlaminar cracks.

During delamination growth new fracture surfaces are continuously created at the crack tip. Let a fixed location in space at an initial distance r from the delamination tip be considered. Fig. 3b shows that if the interlaminar crack length increases by da, then the distance of the aforementioned fixed point must reduce to $r-da$. This also implies that

$$\frac{dD(r)}{dN}=\frac{dD(r)}{dr}\frac{dr}{dN}=-\frac{dD(r)}{dr}\frac{da}{dN} \tag{16}$$

Combining Eqs. (16) and (14) yields

$$\frac{dD(r)}{dr}=\begin{cases}-\frac{[1-D(r)]^{-p}}{(p+1)da/dN}\left[\frac{G_{II\max}}{G_{IIc}}\right]^{\frac{b}{2(1-R)^{\kappa}}} & r\leqslant r_c\\ -\frac{[1-D(r)]^{-p}}{(p+1)da/dN}\left[\frac{G_{II}}{G_{IIc}}\frac{r_c}{r}\right]^{\frac{b}{2(1-R)^{\kappa}}} & r\geqslant r_c\end{cases} \tag{17}$$

Considering the region $0\leqslant r\leqslant r_c$, integrating Eq. (17) with respect to r and finally exploiting the first of the boundary conditions in Eqs. (15) yields

$$[1-D(r_c)]^{p+1}=\frac{r_c}{da/dN}\left[\frac{G_{II\max}}{G_{IIc}}\right]^{\frac{b}{2(1-R)^{\kappa}}} \tag{18}$$

where $D(r_c)$ is the damage value at the edge of the constant shear stress region in the neighbourhood of the interlaminar crack tip.

Similarly, considering the region $r\geqslant r_c$, integrating Eq. (17) with respect to r and employing the second of the boundary conditions in Eqs. (15) leads to

$$1-[1-D(r_c)]^{p+1}=\frac{2r_c(1-R)^{\kappa}}{[b-2(1-R)^{\kappa}]da/dN}\left[\frac{G_{II\max}}{G_{IIc}}\right]^{\frac{b}{2(1-R)^{\kappa}}} \tag{19}$$

Substituting Eq. (18) into Eq. (19) and solving the latter with respect to the delamination growth rate da/dN one gets the fatigue delamination growth law

$$\frac{da}{dN}=r_c\frac{b}{b-2(1-R)^{\kappa}}\left[\frac{G_{II\max}}{G_{IIc}}\right]^{\frac{b}{2(1-R)^{\kappa}}} \tag{20}$$

Eq. (20) is analogous to the one proposed by Andersons et al. [17] in the mode II case for $\kappa=1$.

The mathematical derivation process outlined above proves that Eq. (20) comprises the same fatigue related material parameters as the SN curves given in Eq. (13), i.e. i.e. b and κ. From a physical point of view the material fatigue parameters b and κ must the same for shear driven delamination initiation and propagation since both the processes have been described using the non-linear damage evolution law postulated in Eq. (11). Therefore, once the delamination initiation process has been experimentally characterised, it is then possible to predict the interlaminar crack growth rates using Eq. (20) and vice versa. In any case this implies having to identified experimentally the same two material fatigue parameters which appear in Eq. (11), i.e. b and κ. In the validation of the model which will be carried out in Section 5 b and κ will be estimated by means of delamination initiation tests and then Eq. (20) will be employed to predict delamination growth rate at various stress ratios.

Combining Eq. (18) and (20) the following expression of the damage value at the edge of the constant stress region is obtained

$$D(r_c)=1-\left[1-\frac{2(1-R)^{\kappa}}{b}\right]^{\frac{1}{p+1}} \tag{21}$$

Typically for fibre-reinforced thermoset plastics the exponent b tends to be large, so $b\gg 2(1-R)^{\kappa}$. This implies that Eq. (20) can be approximated as follows

$$\frac{da}{dN}\cong r_c\left[\frac{G_{II\max}}{G_{IIc}}\right]^{\frac{b}{2(1-R)^{\kappa}}} \tag{22}$$

Therefore under the condition $b\gg 2(1-R)^{\kappa}$ the radius of the constant stress region at the delamination tip also represents the pre-factor in the fatigue delamination growth equation. The semi-empirical fatigue delamination growth law given in Eq. (22) is formally analogous to the one proposed by Allegri et al. [25] when $\kappa=2$, with the radius of the constant stress region at the interlaminar crack tip representing the propagation rate pre-factor. For $b\gg 2(1-R)^{\kappa}$ the delamination growth rate versus the normalised ERR curves rotate anticlockwise with increasing R with respect to a pivot point that represents static fracture, as shown in Fig. 2b. In the limit $R\to 1$ such curves become vertical, i.e. there is no stable delamination propagation but only sudden static failure when $G_{II\max}=G_{IIc}$.

Interestingly for $b\gg 2(1-R)^{\kappa}$ one finds $D(r_c)=1$. This result, together with the boundary condition $D(0)=1$ given in the first of Eqs. (15), implies that when the characteristic material fatigue exponent b is sufficiently large, the damage field tends to attain a constant unit value in the constant stress region in the neighbourhood of the delamination tip.

5. Model identification and validation

The model parameters are here identified by means of fatigue delamination onset data at different stress-ratios in double-notch-shear (DNS) specimens obtained by May and Hallett [26,27]. The model validation is then carried out on an independent set of delamination growth data presented by Allegri et al. [25] and obtained from central cut-ply (CCP) specimens [28]. The material considered in all the aforementioned cases is unidirectional IM7/8552, whose mechanical properties are given in Table 1.

5.1. Remarks on DNS testing

The DNS specimen configuration as specified by the ASTM standard [29] and employed in Refs. [26,27] is sketched in Fig. 5. The standard specimen has two half-thickness deep notches arranged

Table 1
material mechanical properties for IM7/8552 [21]; shear strength τ_u from Ref. [22,23]; α_{II} is computed employing the elastic constants given in the table by means of Eqs. (5), (6).

Material	E_x (GPa)	E_z (GPa)	G_{xz} (GPa)	ν_{xz}	G_{IIc} (kJ/m^2)	τ_u (MPa)	α_{II} (1/GPa)
IM7/8552	161	11	5	0.31	1.18	82.5	2.05×10^{-5}

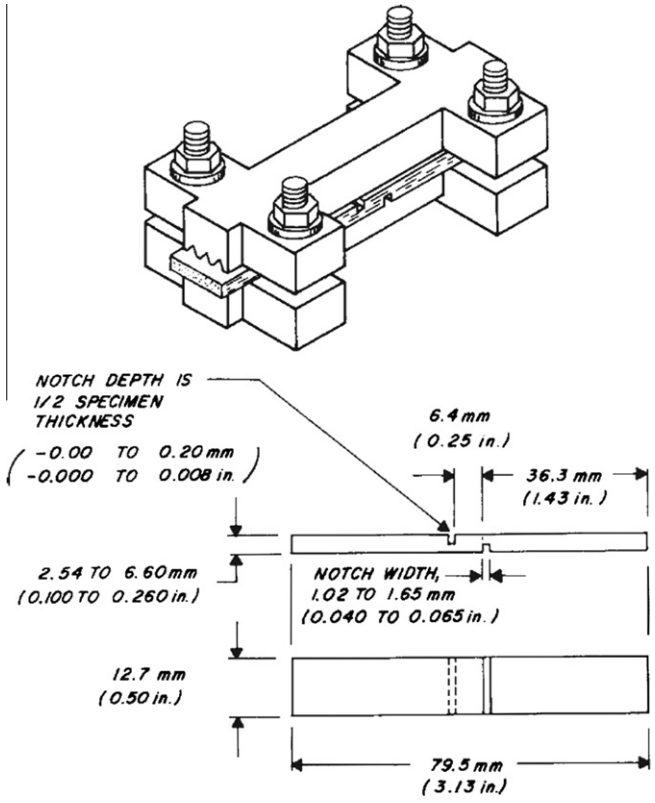

Fig. 5. Standard DNS specimen configuration from ASTM D3846-08 [29].

anti-symmetrically with respect to the longitudinal and transversal mid-planes. The specimen is loaded in compression with anti-bending guides and shear failure occurs along the mid longitudinal plane between the notches. The ASTM D3846 states that the shear strength of the material is obtained from the DNS testing as follows

$$\tau_u = \frac{P_u}{LW} \tag{23}$$

where P_u is the applied compressive force at failure, L is the distance between the notches and W the specimen width; the latter two are strictly prescribed by the ASTM D3846, as shown in Fig. 5. In Ref. [26,27] fatigue tests were performed on DNS specimens using a constant amplitude compressive force with peak amplitude $P_{\max}$ and stress-ratio R. In analogy with Eq. (23), the peak shear stress acting on the longitudinal mid plane between the notches was therefore expressed as follows

$$\tau_{\max} = \frac{P_{\max}}{LW}. \tag{24}$$

It is important to point out that both Eq. (23) and (24) imply that the shear stress is constant along the specimen gauge length, i.e. the longitudinal mid-plane between the notches where failure occurs. Nonetheless, according to the nominal configuration presented in Fig. 5, LEFM dictates that a stress singularity must occur at the notch corners in the DNS specimens [30]. However, for the DNS fatigue specimens considered here, the notch corners bounding the fracture plane had a characteristic fillet radius of about 1 mm; this was because dentist burrs had been used to carve the notches. Linear elastic finite element analyses [31] showed that such fillet radius was sufficient to suppress the shear stress singularity. Moreover it must be considered that the presence of a compressive through-thickness stress enhances the ILSS of fibre-reinforced plastics [32]. When the ILSS enhancement was taken into account in finite element analyses of DNS specimens [27,31], the resulting shear concentration factor at the notch corners was further reduced. This demonstrates that the failure of the DNS specimen is controlled by the interlaminar strength, albeit appropriate shear concentration factors should be accounted for in calculating the actual ILSS from DNS data.

The peak shear stress $\tau_{\max}$ term in Eq. (13) is normalised with respect to the static ILSS τ_u, i.e. the SN curve is expressed in terms of relative load severity. If $\tau_{\max}$ is the nominal stress on the DNS fracture plane and the notched ILSS is employed for τ_u, the left hand side of Eq. (13) will not be affected by the geometrical stress concentration factor K_t associated with the filleted notch corners. Nonetheless, it is well known that the slope of the SN curve may be influenced by the presence of notches [33]. As qualitatively illustrated in Fig. 6, this is because the fatigue notch factor K_f, i.e. the stress concentration factor affecting the endurance limit τ_f, tends to be smaller than the geometrical stress concentration factor K_t. This makes the SN curve shallower by increasing b in Eq. (13). The difference between K_t and K_f is usually accounted for by defining a notch sensitivity factor q as follows [33]

$$q = \frac{K_f - 1}{K_t - 1} \tag{25}$$

which theoretically ranges between zero and one. The notch sensitivity factor depends on the notch radius and the material considered. If the latter is ductile, the q for sharp notches tends to be much smaller than one, whereas brittle materials often have notch sensitivity factors very close to one, usually denoted as "perfect" notch sensitivity [33].

Since epoxy matrixes such as the one considered in this paper are typically brittle at room temperature, it is reasonable to assume that $q \cong 1$, so that from Eq. (25) $K_f = K_t$ and the slope of the SN curve, i.e. the material b exponent, is unaffected by the presence of notches in the DNS specimens. Therefore, for brittle materials, the

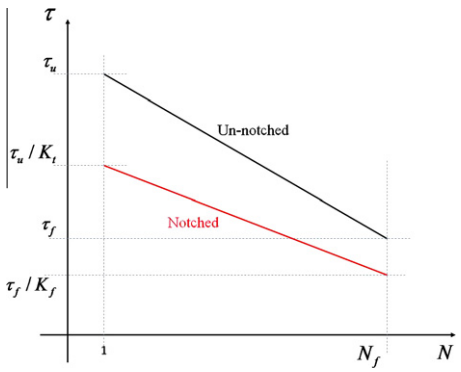

Fig. 6. Qualitative illustration of the effect of notches on SN curves. If $K_f = K_t$ as in brittle materials the un-notched and notched curves will be parallel. If relative severities were plotted on the vertical axis the SN curves will be coincident for brittle materials ("perfect" notch sensitivity case). (For interpretation of the references to colour in this figure legend, the reader is referred to the web version of this article.)

SN curve expressed in terms of severity $\frac{\tau_{max}(x)}{\tau_u}$ as in Eq. (13) is the same for notched and un-notched samples. This is because the definition of severity is independent from the presence of finite stress concentrations and the latter do not influence the slope of the SN curve. This leads to the conclusion that DNS specimens are suitable for charactering the onset of delaminations in fibre-reinforced plastics, provided that the matrix is relatively brittle.

May and Hallett [27] observed that the delamination onset in DNS specimens leads to immediate failure at the candidate fracture plane between the notches concluded that DNS tests provide a robust identification technique for fatigue delamination initiation.

5.2. Model identification via DNS testing

The results of the DNS fatigue initiation tests from Refs. [26,27] are presented in Fig. 7. Three stress-ratios were considered, namely $R = 0.1$, 0.3 and 0.5. It is worth observing that the experimental data present a significant amount of scatter. This is not surprising since the strength of DNS specimens is strongly dependent on several geometric details, such as the depth of the notches [30], whose control during manufacturing represents a significant challenge. Nonetheless general trends are easily identifiable in Fig. 7; in particular the anti-clockwise rotation of the SN curves with increasing stress-ratio can be clearly appreciated. Using Eq. (13), the following model parameters were estimated by a non-linear regression performed over the whole data set with a 95% confidence level

$$b = 10.092 \pm 1.152 \quad \kappa = 2.304 \pm 0.302 \tag{26}$$

The red continuous lines in Fig. 7 represent the model fit, with the dashed lines giving the plus/minus one standard deviation from the mean trends. Eq. (13) correctly reproduces the general trends seen in Fig. 7; the quality of the fit is clearly limited by the significant amount of data scatter in the results.

5.3. Model validation via delamination propagation

The delamination propagation tests considered here are those presented by Allegri et al. [25]. The tests were performed using CCP specimens [28]; these are arranged as unidirectional laminates comprising a given number of ply cuts in the middle. In the configuration considered here, the two central plies were cut out of a total of 10. Under far field tension, delaminations emanate from the layer terminations and they propagate in pure mode II along the interfaces between the cut plies and the continuous ones. In Ref. [25] the delamination growth was monitored using both a high accuracy extensometer and in situ microscopy. The main advantage of the CCP specimen is that it is characterised by a nominally constant ERR as a function of delamination length and this avoids the need for compliance calibration.

The fatigue data set from Ref. [25] is presented in Fig. 8. Again three stress-ratios were considered, namely $R = 0.1$, 0.3 and 0.5. The dashed black line represents the FDG law derived by O'Brien et al. for IM7/8552 using ENF specimens at $R = 0.1$ [34]. It is worth observing that such data agree well with those generated using CCP specimens at the same stress-ratio and this proves the suitability of CCP specimens for FDG characterisations of fibre-reinforced plastics. The red continuous lines represent the delamination growth rates predicted using Eq. (20) together with the model parameters in Eq. (26), which have been identified via fatigue initiation tests on DNS specimens. The dashed lines represent the plus/minus one standard deviation trends from the average delamination growth rate predictions.

From Fig. 8 one can observe that employing Eq. (20) in conjunction with the model parameters estimated from SN curves gives a good prediction of the delamination growth rates for the $R = 0.3$ and $R = 0.5$ cases, while the delamination propagation rates are overestimated for $R = 0.1$. However in this case the prediction is conservative. The anticlockwise rotation of the experimental delamination growth data with respect to the stress-ratio value can be easily appreciated in Fig. 8. This is well captured in terms of average trends by Eq. (20).

It is worth observing the lines representing the model predictions intersect at almost exactly the same point on the chart. This is due to the fact that in the case of IM7/8552 b is large enough for Eq. (20) to be well approximated by Eq. (22). In other words the fatigue delamination growth equations given in Eqs. (20) and (22) predict that when the mode II ERR approaches the mode II fracture toughness, the delamination size increases at a speed approximated by the characteristic length r_c per unit cycle. However this is an underestimation of the actual growth rate for $G_{II} \to G_{IIc}$, since in such regime the experimental evidence proves that delamination propagation becomes unstable and so $\frac{da}{dN}$ should diverge [35].

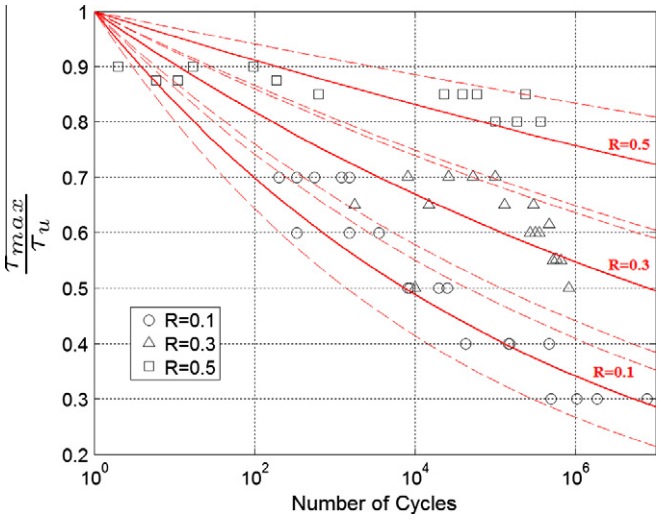

Fig. 7. SN curves for DNS specimens [26,27]. Eq. (13) in red continuous line; one standard deviation bands in red dashed lines. (For interpretation of the references to colour in this figure legend, the reader is referred to the web version of this article.)

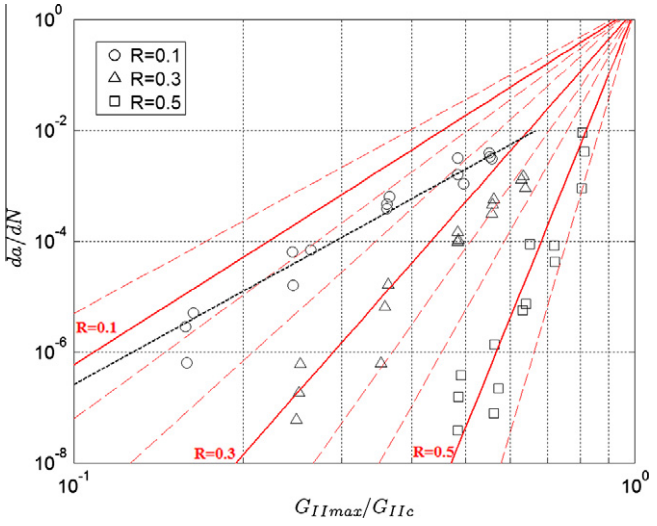

Fig. 8. delamination propagation data from Ref. [25]. Predictions from Eq. (20) in red continuous lines; one standard deviation bands in red dashed lines. Paris fit of FDG data from Ref. [34] in black dashed line. (For interpretation of the references to colour in this figure legend, the reader is referred to the web version of this article.)

Nonetheless Fig. 8 demonstrates that Eq. (20) and (22) are adequate for describing the fatigue delamination propagation in the "stable growth regime" [35], i.e. when $\frac{da}{dN}$ can be described via a power law of the ERR attained at the crack tip.

This implies that employing Eq. (22) should suffice in most practical cases. As a further evidence of this conclusion it should be observed that Allegri et al. [25] have demonstrated that a constant pre-factor equation formally analogous to Eq. (22) is suitable for describing the stress-ratio effect on fatigue delamination growth in a wide range of fibre-reinforced toughened epoxies.

6. Conclusions

A novel non-linear damage evolution model for describing both the onset and propagation of mode II delaminations in fibre-reinforced laminates under constant amplitude loading has been presented and validated. This makes it possible to predict the propagation behaviour of delaminations from initiation data and vice versa. The unification of these phenomena that are normally treated independently offers the prospect of simplifying analysis and design methods and reducing the amount of testing necessary to characterise delamination fatigue behaviour. The approach is based on defining a scalar damage variable that represents the spent fraction of the fatigue endurance of ply interfaces and on postulating a general damage evolution law as function of the number of cycles, peak stress and stress-ratio.

The integration of the damage evolution law yields an equation representing SN curves which rotate with respect to a pivot point which identifies static fracture. Exploiting a non-singular expression of the shear stress at the delamination tip originally proposed by Mandell and Meier [16], it is possible to derive a law describing the propagation rate of an interlaminar crack as a function of the ERR. This law has a strong similarity with other semi-empirical delamination propagation equations already proposed in the literature [7,25], which have been proven valid for several fibre-reinforced toughened epoxies. Both the onset and propagation equations are based on the same two fatigue related material dependant parameters. The approach described above has been validated by means of DNS endurance data for initiation and CCP propagation data for delamination growth. The model predictions were in good agreement with the experimental data, albeit on the conservative side for the propagation tests at $R = 0.1$.

Acknowledgement

The authors are grateful to Rolls-Royce Plc for having supported this research through the Composites University Technology Centre at the University of Bristol.

Appendix A. Linear damage accumulation for non-linear damage evolution

Let x be an arbitrary location within a pristine interface subjected to a local shear stress $\tau_{\max}(x)$. The damage field defined in Eq. (10) has local value $D(x)$. Non-linear damage evolution models with separable variables can be expressed in the following form

$$\frac{dD(x)}{dN} = f[D(x)]g\left[R, \frac{\tau_{\max}(x)}{\tau_u}\right] \tag{A.1}$$

where f and g are suitable continuous functions. Comparing Eq. (11) to Eq. (A.1) immediately proves that the former has separable variables. For the sake of simplifying the notation the x dependency will be dropped since the following derivation is carried out at a fixed location in space. Let $\frac{\tau_{\max i}}{\tau_u}$ and R_i respectively be the load severity and stress-ratio applied for a certain number of cycles ΔN_i at the location x. In order to evaluate ΔN_i, one must separate the variables in Eq. (A.1) and integrate with respect to the damage increment $\Delta D_i = D_{i+1} - D_i$ which follows the application of ΔN_i load cycles. Proceeding as stated one finds

$$\Delta N_i = \left[g(R_i, \frac{\tau_{\max i}}{\tau_u})\right]^{-1} \int_{D_i}^{D_{i+1}} \frac{dD}{f(D)} \tag{A.2}$$

On the other hand the number of cycles to complete failure at the location x at the same load severity and stress-ratio is given by

$$N_{fi} = \left[g(R_i, \frac{\tau_{\max i}}{\tau_u})\right]^{-1} \int_0^1 \frac{dD}{f(D)} \tag{A.3}$$

By virtue of the additive property of integrals and exploiting Eq. (A.2) one can write

$$\int_0^1 \frac{dD}{f(D)} = \sum_{i=1}^{m} \int_{D_i}^{D_{i+1}} \frac{dD}{f(D)} = \sum_{i=1}^{m} g\left(R_i, \frac{\tau_{\max i}}{\tau_u}\right)\Delta N_i \tag{A.4}$$

where m represents the number of "blocks" having given constant severity and stress-ratio that are comprised in the complete load history.

On the other hand, from Eq. (A.3) one has

$$g\left(R_i, \frac{\tau_{\max i}}{\tau_u}\right) = \frac{1}{N_{fi}} \int_0^1 \frac{dD}{f(D)} \tag{A.5}$$

Substituting Eq. (A.5) into Eq. (A.4) leads to

$$\sum_{i=1}^{m} \frac{\Delta N_i}{N_{fi}} = 1 \tag{A.6}$$

which is the well known Miner's linear damage accumulation rule.

References

[1] Degrieck J, Van Paepegem W. Fatigue damage modelling of fibre-reinforced composite materials: a review. Appl Mech Rev 2001;54(4):279–300.
[2] O'Brien TK. Characterization of delamination onset and growth in a composite laminate. In: damage in composite materials. ASTM STP 1982;775:140–67.
[3] O'Brien TK. Towards a damage tolerance philosophy for composites materials and structures. In: composite materials: testing and design (IX volume). ASTM STP 1990;1059:7–33.
[4] O'Brien, TK. Development of a composite delamination fatigue life prediction methodology. NASA, Report LF99-9386; 2009.
[5] ASTM D6115-97. Standard test method for mode i fatigue delamination growth onset of unidirectional fiber-reinforced polymer matrix composites. ASTM; 2004.
[6] Curtis PT. The fatigue behaviour of fibrous composite materials. J Strain Anal Eng Design 1989;24:235–44.
[7] Kun F, Carmona HA, Andrade JS, Herrmann HJ. Universality behind Basquin's law of fatigue. Phys Rev Lett 2008;100:094301.
[8] Degrieck J, Van Paepegem W. Fatigue damage modelling of fibre-reinforced composite materials: review. Appl Mech Rev 2001;54(4):279–300.
[9] Sidoroff F, Subagio B. Fatigue damage modelling of composite materials from bending tests. In: Matthews FL, Buskell NCR, Hodgkinson JM, Monton J, editor. IV Int. conf. on composite materials, (ICCM-VI) & second European conference on composite materials (ECCCM-11), proceedings, vol. 4. London, UK: Elsevier, 20–24 July 1987. p. 432–39.
[10] Vieillevigne S, Jeulin D, Renard J, Sicot N. Modelling of the fatigue behaviour of a unidirectional glass epoxy composite submitted to fatigue loadings. In: Degallaix S, Bathias C, Fougères R, editor. Int. conf. on fatigue of composites. Proc., 3–5 June 1997, Paris, France, La Société Française de Métallurgie et de Matériaux; 1997. p. 424–30.
[11] Kawai M. Damage mechanics model for off-axis fatigue behaviour of unidirectional carbon fibre-reinforced composites at room and high temperatures. In: Massard T, Vautrin A, editor. Proc. of 12th int. conf. on composite materials (ICCM-12), Paris, France, 5–9 July 1999. p. 322–29.
[12] Bergmann HW, Prinz R. Fatigue life estimation of graphite/epoxy laminates under consideration of delamination growth. Int J Numer Methods Eng 1989;27:323–41.
[13] Dahlen C, Springer GS. Delamination growth in composites under cyclic loads. J Compos Mater 1994;28:732–81.
[14] Schon J. A model of fatigue delamination in composites. Compos Sci Technol 2000;60:553–8.
[15] Allen DH, Harris CE, Groves SE. A thermomechanical constitutive theory for elastic composites with distributed damage—I. Theoretical development. Int J Solids Struct 1987;23:1301–18.

[16] Mandell JF, Meier U. Fatigue crack propagation in 0°/90° e-glass/epoxy composites, fatigue of composite material. ASTM STP 1975;569:28–44.
[17] Andersons J, Hojo M, Ochiai S. Model of delamination propagation in brittle-matrix composited under cyclic loading. J Reinforced Plast Compos 2001;20(5):431–50.
[18] Sih GC, Paris PC, Irwin GR. On cracks in rectilinearly anisotropic bodies. Int J Fracture Mech 1965;1(3):189–203.
[19] Suo Z, Bao G, Fan B, Wang TC. Othotropy rescaling and implication for fracture in composites. Int J Solids Struct 1991;28(2):235–48.
[20] O'Brien TK. Composite Interlaminar shear fracture toughness G_{IIc}: shear measurement or sheer myth, composite materials: fatigue and fracture, VII ed. ASTM STP 1998;1330:3–18.
[21] Chaboche JL. Continuum damage mechanics: Part I – general concepts. ASME J Appl Mech 1988;55(1):59–64.
[22] Lemaitre J, Desmorat E. Engineering damage mechanics: ductile, creep, fatigue and brittle failures. Springer; 2005.
[23] Chaboche JL, Lesne PM. A non-linear continuous fatigue damage model. Fatigue Fract Eng Mater Struct 1988;11(1):1–17.
[24] Chen HS, Hwang SF. Accelerated fatigue properties of unidirectional carbon/epoxy composite materials. Polym Compos 2006;27(2):138–46.
[25] Allegri G, Jones MI, Wisnom MR, Hallett SR. A new semi-empirical model for stress-ratio effect on mode II fatigue delamination growth. Composite Part A 2011;42(7):733–40.
[26] May M, Hallett SR. Analysis of damage evolution in unidirectional carbon/epoxy samples under shear fatigue loading. In: 17th International conference on composite materials, 27–31 July, 2009, Edinburgh, UK.
[27] May M, Hallett SR. An assessment of through-thickness shear tests for initiation of fatigue failure. Compos Part A: Appl Sci Manuf 2010;41(11):1570–8.
[28] Wisnom MR, Jones MI, Cui W. Delamination in composites with terminating internal plies under tension fatigue loading. In: Composite materials: fatigue and fracture (V volume), ASTM STP 1239, 1995. p. 486–508.
[29] ASTM D3846-08. Standard test method for in-plane shear strength of reinforced plastics, volume 8.02, ASTM Standards; 1995. p. 435–9.
[30] Shokrieh MM, Lessard LB. An assessment of the double-notch shear test for interlaminar shear characterization of a unidirectional graphite/epoxy under static and fatigue loading. Appl Compos Mater 1998;5(5):298–304.
[31] Allegri G, May M, Hallett SR. On the effect of interlaminar compressive stresses in double-notch shear specimens. In: Proceedings 14th European conference on composite materials, Budapest, Hungary, 2010.
[32] Li X, Hallett SR, Wisnom MR. Predicting the effect of through-thickness compressive stress on delamination using interface elements. Compos Part A: Appl Sci Manuf 2008;39(2):218–30.
[33] Bandhari VB. Design of machine elements. Sec. 8, 154. Mc Graw-Hill; 2010 [chapter 5].
[34] O'Brien TK, Johnston WM, Toland GJ. Mode II interlaminar fracture toughness and fatigue characterization of a graphite epoxy composite material. NASA/TM-2010-216838, 2010.
[35] Trethewey BR, Gillespie JW, Carlsson LA. Mode II cyclic delamination growth. J Compos Mater 1988;22:459–83.